ARCHITECTURE CIVIL ENGINEERING ENVIRONMENT
The Silesian University of Technology
No. 3/2022

doi: 10.2478/ACEE-2022-0031

# ROLE OF THERMAL ENERGY STORAGE TECHNOLOGY IN THE DECARBONIZATION OF ENERGY SECTOR PROCESS – PACKED ROCK BED PARAMETERS ANALYSIS

Jakub OCHMANN [a*], Michał JURCZYK [b], Łukasz BARTELA [c]

[a] MSc; Silesian University of Technology, Department of Power Engineering and Turbomachinery, Konarskiego 18, 44-100 Gliwice, Poland
*Corresponding author. E-mail address: *jakub.ochmann@polsl.pl*

[b] PhD; Silesian University of Technology, Department of Power Engineering and Turbomachinery, Konarskiego 18, 44-100 Gliwice, Poland

[b] DSc; Silesian University of Technology, Department of Power Engineering and Turbomachinery, Konarskiego 18, 44-100 Gliwice, Poland

Received: 15.03.2022; Revised: 17.05.2022; Accepted: 24.05.2022

Abstract
**The paper presents the adiabatic installation of compressed gases energy storage. The authors present the results of analyzes for this type of installation due to the selection of thermal storage material. The simulations were carried out for basalt, granite and ceramics (alumina) as well as for porosity value from 0.375 to 0.39 of basalt-filled reservoirs in Thermal Energy Storage (TES) installation. Characteristics of outlet air temperature, air pressure drop amount of energy stored and external heat losses as a time functions during the charging phase are presented. The research indicated that due to the lowest density and average heat capacity of the materials studied, granite has the fastest and most intense physical exit loss from the storage tank which was approximately 1100 W. However, there was no significant effect on air pressure drop depending on the chosen accumulation materials. The effect of rock bed porosity on the pressure drop of flowing air was investigated. For a constant mass flow rate, pressure drop values ranging from 2200 Pa to 6200 Pa were obtained depending on the porosity value.**

Keywords: **Packed bed; Thermal energy storage; ANSYS Fluent; CFD; Adiabatic CAES.**

## LIST OF SYMBOLS:

| | |
|---|---|
| $\alpha$ | permeability coefficient, $m^2$, |
| $\Delta p$ | air pressure drop, Pa, |
| $\varepsilon$ | average porosity of packed bed, -, |
| $\rho$ | density of air, $kg/m^3$, |
| $\mu$ | viscosity of air, Pa·s, |
| $A_{fs}$ | specific surface area, 1/m, |
| $C_2$ | inertia loss coefficient, 1/m, |
| $D_p$ | rock particles diameter, m, |
| $E_f$ | total fluid energy, J, |
| $E_s$ | total solid energy, J, |
| $h_{fs}$ | heat transfer coefficient, $W/m^2K$, |
| $h_{ex}$ | external heat transfer coefficient, $W/m^2K$, |
| $k_f$ | fluid thermal conductivity, W/m·K, |
| $L$ | length of TES tank, m, |
| $N_u$ | Nusselt number, -, |
| $Nu_{ex}$ | Nusselt number for external convection, - |
| $Pr$ | Prandtl number, -, |

| | |
|---|---|
| *Ra* | Rayleigha number, -. |
| *Re* | Reynolds number, -, |
| $S_f^h$ | fluid enthalpy source term, J/kg, |
| $S_s^h$ | solid enthalpy source term, J/kg, |
| $T_f$ | temperature of fluid, K, |
| $T_s$ | temperature of solid, K, |
| t | time, s, |
| $v_\infty$ | velocity of air, m/s, |

## 1. INTRODUCTION

The global energy sector is currently at the stage of far-reaching changes. In order to reduce the emission of pollutants to the atmosphere, soil or water resulting from the production of electricity, the importance of renewable energy sources (RES) in the global energy mix is growing [1].

Due to the decarbonization process, fewer and fewer high-power central generating units are created. These units generate electricity by converting fossil fuels such as hard coal, lignite and natural gas and this process is accompanied by a significant emission of harmful substances. On the opposite extreme, there are renewable energy sources. In 2020 a record share of RES in the global energy mix was noted – about 29% [2]. A significant trend of increasing importance of renewable energy sources in energy systems is also visible in Poland. In 2018, the installed capacity in RES accounted for 14.41% of the structure of the National Energy System, while in 2020 this value was 20.78% [3]. Renewable energy sources are mainly wind farms and photovoltaic power plants. RES installations, such as wind turbines and solar panels, are characterized by a variation in the amount of electricity produced mainly due to their dependence on the current weather conditions [4, 5]. Additionally, there are changes in power demand in the power grid related to the variable activity of electricity consumers during a day [6]. In order to stabilize power grids, it is necessary to use additional elements of power systems. This can be done by energy storage installations. These installations store the surplus of electricity when there is an excess of it in the power grid and return electricity to the grid when demand increases [7]. Pumped-hydro storage (PHS) is well known and commercially available as well as the most commonly used technology for energy storage [8]. However, this technology also has its limitations. There are alternatives to using PHS as energy storage. One of them is the use of hydrogen produced in the electrolysis of water as an energy carrier [9, 10]. Another solution is CGES (Compressed Gases Energy Storage) system. In this energy storage technology, the energy carrier is gas - most often atmospheric air (Compressed air Energy Storage – CAES) or carbon dioxide. The scheme of basic CAES installation is presented in Fig. 1.

The world's first CAES system was build in Germany. The Huntorf power plant has been operating since 1978. The compressed gas is stored in two salt caverns by total volume over 170,000 m$^3$, which are located 600 m below ground level. Maximum pressure of stored gas is equal 70 bar. The CAES system in Huntorf operates with an efficiency of about 42% [11, 12, 13]. The

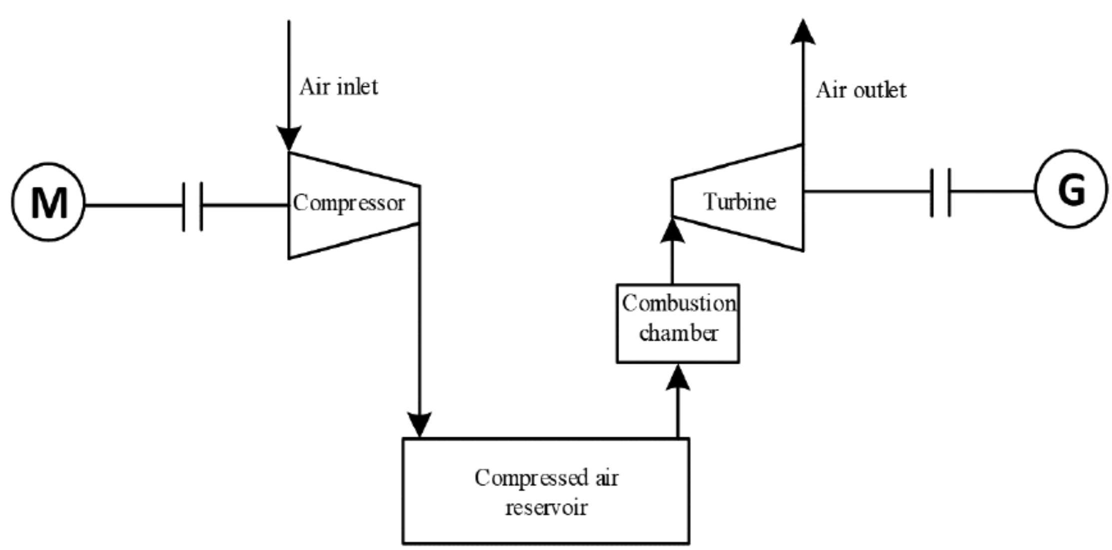


**Figure 1.**
**The scheme of basic CAES installation**

next CAES system was built in Alabama in 1991. In McIntosh power plant salt cavern is located 500 m below ground and is characterized by total volume over 500,000 $m^3$. The gas reservoir can store compressed air between 46 and 74 bar. Compared to the Huntorf power plant, the McIntosh installation uses several improvements, which allows it to achieve an efficiency of 54% [13]. Both described installations are an example of conventional diabetic compressed air systems (D-CAES) using fossil fuels to heat the air before the process of its expansion on the turbine. However, the basic CGES system, like diabatic CAES installations, does not solve the problem of managing the waste heat generated in the gas compression process, as a result of which it is lost. The expanded air can be heated with use of combustion chambers powered by natural gas but this is contradict to the idea of storing green energy due to the introduction of an additional source of exhaust emissions into the atmosphere. There are numerous modifications to the compressed gases energy storage systems in order to increase the environmental friendliness and efficiency of the system. Considered are, among others, Thermal Energy Storage (TES) installations, which use buffers to accumulate the heat generated in the gas compression process and storing it until it is received by the expanded air. The use of a heat buffer in the compressed gas storage process is called as adiabatic CGES system. The TES systems can be based on different heat storage materials like phase change materials (PCM), solid materials or thermal oil. Systems that are based on thermal oil circulation or phase change materials are also often used in cooperation with solar plants [14, 15]. The authors in reference [16] present the results of the research for a solar air heater using straight and spiral absorber tubes with TES system. The experimental study of a solar air heater was studied for an aluminum absorber, spiral coil and straight tubes filled with glycerol and PCM . The studies were conducted under natural circulation at a constant mass flow rate of air. As a result, the maximum thermal and exergy efficiencies were obtained by authors for a spiral coil with short-time heat storage. Another example of TES can be the solution described by the authors in reference [17], where study to enhance the performance of commercial PTC (Parabolic Trough Collector) concentrated solar thermal power plants with thermal energy storage capability are presented. The authors proposed to combine the TES and Concentrated Solar Power (CSP) with the steam-based Rankine cycle systems. An application of solar air heater with Thermal Energy storage was shown by authors in reference [18]. Another point of view is shown by the authors in reference [19]. The paper shows a broad overview of PCM technologies that can also be applied to increase the energy efficiency of buildings, allowing for a completely new application of the described TES technology. This shows that this technology can not only be used in large-scale energy storage processes in energy systems, but also contribute to the storage of heat in buildings on a smaller scale. During the decarbonization process and reducing the importance of fossil fuel-based production units, it is also important to properly allocate post-mining shafts. The process of decommissioning such a post-mining shaft is extremely costly, and the shaft itself still requires constant control and supervision of methane utilization [20, 21]. The use of post-mining shafts as an underground compressed air reservoir is a chance to utilize unused underground and above-ground post-mining infrastructure, as well as expand the power grid with large-scale electricity storage systems.

Also adiabatic CAES (A-CAES) installations that can use one of the heat storage methods within the system can also have a higher efficiency then the diabatic installations – about 70%, [22]. As shows the research presented by the Authors in [23] the encapsulated phase change materials showed great improvement in recovering heat from the high temperature air and can improve A-CAES installation efficiency. The scheme of Thermal Energy Storage installation with packed rock bed is shown in Fig. 2.

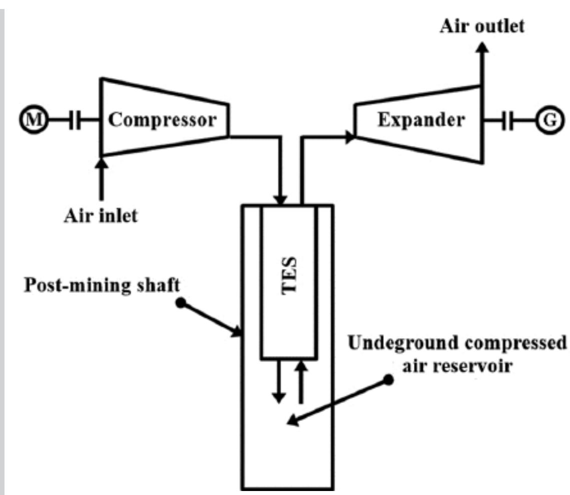


**Figure 2.**
**The scheme of adiabatic CGES system**

The paper presents the adiabatic installation of compressed gases energy storage [24]. The authors present the results of analyzes for this type of installation

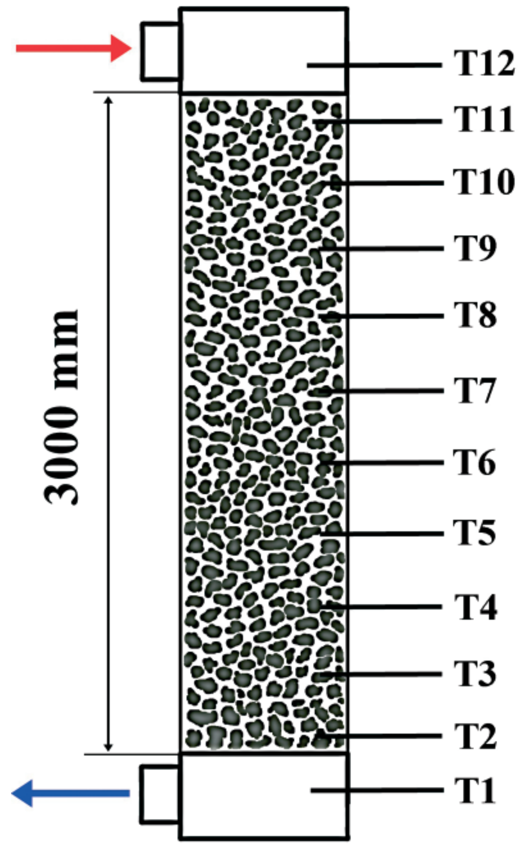


**Figure 3.**
**The laboratory bench of TES installation**

due to the selection of thermal storage material. The simulations were carried out for basalt, granite and ceramics (alumina) as well as for different porosity value of basalt-filled reservoir in TES installation. Characteristic of outlet air temperature, air pressure drop amount of energy stored and external heat losses as a time functions during the charging phase are presented.

## 2. METHODS AND MATERIALS

The experimental research was entirely performed by using the infrastructure of the Silesian University of Technology. Packed bed performance studies were conducted on a laboratory scale Thermal Energy Storage stand located in the Department of Power Engineering and Turbomachinery. The laboratory bench is presented in Fig. 3.

The 3 meter high DN219 Thermal Energy Storage tank with its slenderness reflects the system that could potentially be installed in a mine shaft. The tank has a wall thickness of 3 mm and is made of stainless steel with a temperature dependent thermal conductivity of 14.1–18.3 W/mK [25]. Basalt grit with an average diameter of 15.5 mm was selected as the tank fill material. Calculations indicated that the porosity of the rock deposit, defined as the ratio of air spaces to rock material, is approximately 0.38. In addition, the measurement system allows real-time tracking of the temperature of the rock material using resistance temperature detectors (T2 – T11) and the value of the pressure drop of the air flowing through the storage tank.

ANSYS Fluent software was used to simulate the heating process of a rock material in a Thermal Energy Storage tank with a geometry equivalent to a laboratory scale heat storage tank. The heat transfer between air and rock material is determined by the heat transfer coefficient $h_{fs}$, which can be defined as [26, 27]:

$$h_{fs} = \frac{Nu \cdot k_f}{D_p} = \frac{(2 + 1{,}1 \cdot Re^{0{,}6} \cdot Pr^{1/3}) \cdot k_f}{D_p} \quad (1)$$

The values of Reynolds number *Re* and Prandtl number *Pr*, as well as the value of air heat conductivity coefficient $k_f$, are variable values during the process. In order to be more accurate, a UDF file was implemented so that the value of heat transfer coefficient $h$ is calculated in real time of the simulation. The Porous Zone Model and the Non-Equilibrium Thermal Model were used to simulate the rock deposit. The result is the division of the computational domain into two overlapping zones: the fluid flow zone and the rock material zone. This results in the simulation of heat transfer between air and rock material based on temperature differences recorded at the nodes of the numerical grid. The conservation equation solution is also separated. The conservation equation solved for the fluid zone is defined as:

$$\frac{\partial}{\partial t}(\varepsilon \rho_f E_f) + \nabla \cdot \left(\vec{v}(\rho_f E_f + p)\right) = \nabla \cdot \left(\varepsilon k_f \nabla T_f - \left(\sum_i h_i J_i\right) + (\bar{\bar{\tau}}_{=})\right) + + S_f^h + h_{fs} A_{fs} (T_s - T_f) \tag{2}$$

The conservation equation solved for the solid zone is defined as:

$$\frac{\partial}{\partial t}((1-\varepsilon)\rho_s E_s) = \nabla \cdot ((1-\varepsilon) k_s \nabla T_s) + + S_s^h + h_{fs} A_{fs} (T_f - T_s) \tag{3}$$

A porous bed is characterized by its individual permeability, which depends on the porosity value, the shape of the individual bed elements or their size. The fluid flow through the bed causes a pressure drop, for the calculation of which it is necessary to define the value of permeability coefficient α and inertial resistance factor $C_2$:

$$\alpha = \frac{{D_p}^2}{150} \cdot \frac{\varepsilon^3}{(1-\varepsilon)^2} \tag{4}$$

$$C_2 = \frac{3.5}{D_p} \cdot \frac{(1-\varepsilon)}{\varepsilon^3} \tag{5}$$

The value of the pressure drop of air flowing through the heat storage tank is determined by Ergun's equation:

$$\frac{|\Delta p|}{L} = \frac{150 \cdot \mu}{D_p^2} \cdot \frac{(1-\varepsilon)^2}{\varepsilon^3} \cdot v_\infty + \frac{1.75 \cdot \rho}{D_p} \cdot \frac{(1-\varepsilon)}{\varepsilon^3} \cdot v_\infty^2 \tag{6}$$

The Ergun equation is applicable for wide ranges of operating pressures of the flowing medium [23]. This is achieved by taking into account the density and viscosity parameters as well as the flow velocity through the porous bed. A study has been undertaken on air pressure drop for large-scale adiabatic CAES heat storage systems [28]. Despite the high air pressure, due to the larger diameter of the storage tank and consequently the lower flow velocity, the air pressure drop value did not exceed 2.5 kPa.

Samples of basalt grit, which is the fill of the TES heat storage tank, were tested using thermal methods to determine the thermodynamic properties of the material. The thermal conductivity coefficient of the rock material and its heat capacity were determined with the TCi analyzer made by C-Therm using the MTSP technique [29]. The obtained values were compared with literature data and introduced into ANSYS Fluent [30], depending on the temperature of the rock material, which further increases the accuracy of the calculations. The studied basalt samples are presented in Figure 4.

**Figure 4.**
**The studied basalt samples**

A key aspect in the operation of a single-phase rock-filled TES heat storage tank is the proper selection of the storage material with consideration of thermophysical values. Maximum operating temperature, defined as the temperature in cyclic operation at which internal structural changes in the rock material do not occur, which could lead to e.g. increased brittleness of the material and consequent destruction of the rock deposit in the lower layers of the packed bed. The thermal conductivity coefficient of the packed-bed material affects the energy dispersion within the rock material during the heat storage phase. If the coefficient is high, energy flows from

**Table 1.**
**The obtained and assumed parameters of the investigated materials in TES installation**

| Item | Basalt | Granite | Ceramics – alumina | Unit |
|---|---|---|---|---|
| Density | 2660 | 2400 | 3960 | kg/m$^3$ |
| Heat capacity | 870–922 | 810–840 | 766–962 | J/kg·K |
| Thermal conductivity | 2.1–2.3 | 1.9–2.1 | 24.5–32.8 | W/m·K |
| Max. operating temperature | ~700 | 650 | 1600 | °C |

**Table 2.**
**The studied values of particle diameters and porosity for analyzed samples of materials in TES installation**

| Item | No. 1 | No. 2 | No. 3 | No. 4 | Unit |
|---|---|---|---|---|---|
| Particle diameter $D_p$ | 24.5 | 20 | 15.5 | 12 | mm |
| Porosity $\varepsilon$ | 0.39 | 0.385 | 0.38 | 0.375 | - |

areas of higher energy density to colder regions. In this scenario, while there is no energy loss to the environment, there is an exergy loss effect through a decrease in the stored energy potential [31]. The obtained and assumed parameters of the investigated materials are shown in Table 1 [32].

In addition, the dependence of the performance of a basalt-filled heat storage tank on the porosity value of the rock bed was investigated. It was assumed that there is a relationship between the average diameter of the rock element and the porosity value. Lower element diameter leads to more efficient filling of voids, so that with decreasing diameter the porosity value also decreases. The studied values are shown in Table 2.

The value of element diameter $D_p$ and porosity $\varepsilon$ directly affect the value of air pressure drop (Eq. 2). The external heat transfer coefficient $h_{ex}$ determines the intensity of energy loss from the storage tank to the environment. Due to the experimental conditions (i.e., no mechanical ventilation of the room, no cooling fans), it is presumed that natural convection is the heat transfer mechanism between the external wall of the storage tank and the environment. The correlation on external Nusselt number, which was proposed by Churchill and Chu, was used to determine the $h_{ex}$ value [33]

$$Nu_{ex} = 0.68 + \frac{0.503 \cdot Ra^{1/4}}{\left[1 + \left(\frac{0.492}{Pr}\right)^{9/16}\right]^{4/9}} = \frac{h_{ex} \cdot L}{k_f} \qquad (7)$$

Calculations were performed with the boundary conditions shown in Table 3.

**Table 3.**
**The boundary conditions for the rock deposit in TES installation**

| Item | Value | Unit |
|---|---|---|
| Inlet air temperature | 80 | $^{o}$C |
| Inlet air mass flow | 0.04 | kg/s |
| Ambient temperature | 20.1 | $^{o}$C |
| Ambient pressure | 101325 | Pa |
| Average external heat transfer coefficient | 5 | W/m$^2$K |

## 3. RESULTS

Based on the experiments and validation of the numerical model, a satisfactory level of agreement between empirical and computational results was achieved. Example comparison of air pressure drop and basalt temperature functions are presented in Fig. 5.

As indicated in Fig. 5, the air pressure drop was studied as a function of different mass fluxes. It was demonstrated that there is a constant difference between the simulation and experimental results of about 100 Pa, however, this difference is insignificant. The curves representing the temperature increase of the rock bed at individual points (marked in Figure 5) also showed differences in the results, however, these are within acceptable limits of agreement.

The first part of the research concerned the development of performance characteristics of the Thermal Energy Storage tank depending on the filling material, assuming identical porosity of the rock bed and size of the rock elements. The presented characteristics were developed for the charging phase of the energy storage tank for material properties indicated in Table 1 and the boundary conditions indicated in Table 3.

Fig. 6 presents characteristics of temperature of out-

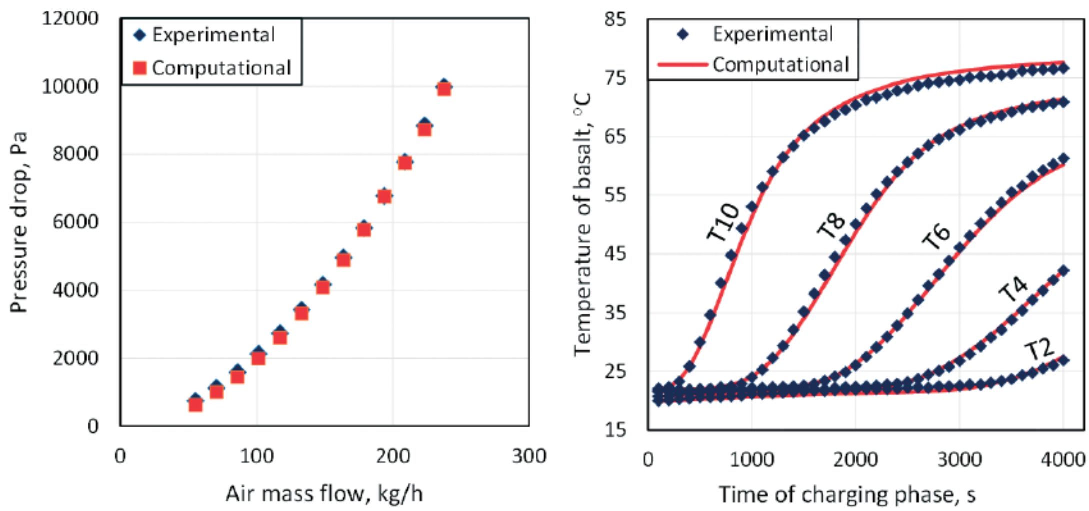


**Figure 5.**
**Example comparison of air pressure drop (left) and basalt temperature (right) functions**

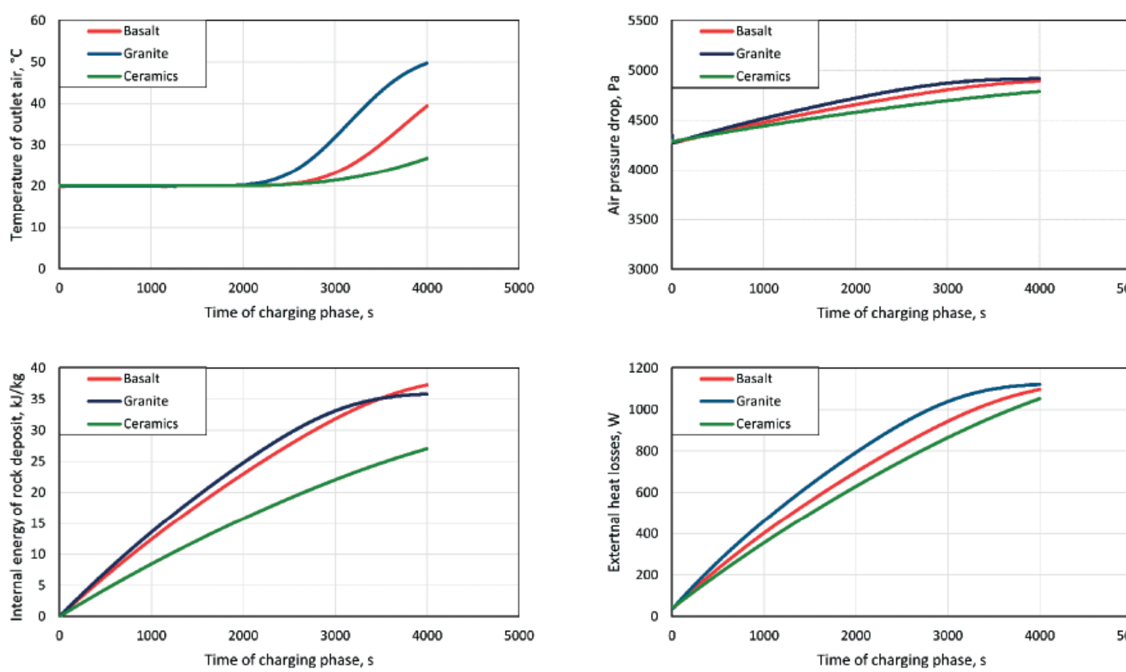


**Figure 6.**
**Characteristic of temperature of outlet air, air pressure drop, internal energy of rock deposit and external heat losses as a time functions for the investigated materials in TES installation**

let air, air pressure drop, the internal energy of rock deposit and external heat losses as a time functions for the investigated materials in TES installation.

The study indicated (Fig. 6) that the earliest and fastest increase in outlet temperature from the TES tank was observed for the granite fill. The least intense rise was recorded for ceramic fill. This is a direct result of the lowest density of granite, which results in a lower mass of material needed for heating and relatively low heat capacity. The differences in the air pressure drop are insignificant and are due to the different degrees of charging of the storage tank in the studied time range, which affects the airflow velocity and density (Eq. 2). Therefore, it can be concluded that the type of heat storage filling does not affect the maximum air pressure drop, but only the intensity of its increase in time. The internal energy increment is most intense in the granite-filled tank,

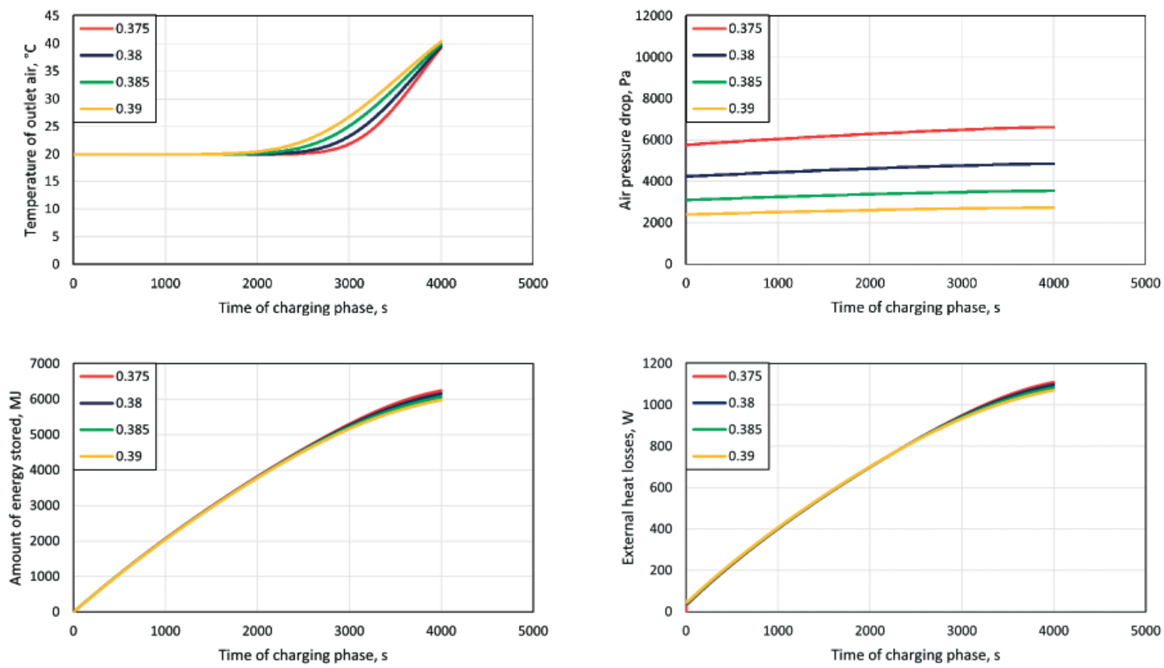


**Figure 7.**
**Characteristic of outlet air temperature, air pressure drop amount of energy stored and external heat losses as a time functions during the charging phase for different porosity value of basalt-filled reservoir in TES installation**

and around 3500 seconds of the charging phase, there is a decrease in the intensity of this increment, suggesting a high degree of charging of this tray has been achieved. The slowest increase in energy stored in the ceramic material is the result of the lower value of the heat transfer coefficient (Eq. 1) between air and solid material resulting from the lower air velocity and the much higher material density indicated in Table 1. Investigations performed in terms of heat loss to the environment through the side surface of the heat storage tank indicated that the highest heat loss was achieved by the granite-filled tank, however, the curve of the ceramic-filled tank indicates relatively high losses of this case, which may be caused by the clearly higher heat conduction coefficient of ceramic compared to this parameter of basalt or granite.

The second part of the research was based on a basalt-filled reservoir (due to the possibility of comparing the results with the planned experimental studies), in which the porosity value of the rock bed and the average diameter of the rock material were parameterized. In fact, the value of porosity is variable and individual in the volume of the rock deposit depending on the intensity of the backfill, the proximity of the bed boundary walls or the irregularity of the bed particles. The tested values of bed element diameters and bed porosity are indicated in Table 2.

Figure 7 shows the increase in outlet air temperature during the charging phase of the heat storage tank, air pressure drop, amount of energy stored and external heat losses as a time functions for different porosity values of basalt-filled reservoir in TES installation.

The results showed that as the porosity value increases, the air temperature rise occurs faster but with less intensity than for the lowest porosity value. The porosity value directly affects the mass of rock material stored in the heat storage volume. A higher porosity value results in less rock material requiring heating - the effect of which can be seen in Figure 6 as an early rise in outlet air temperature. A noticeable difference in the results of the pressure drop of air flowing through the tank calculated by Equation 2 are also shown in Fig. 6. Decreasing porosity increases the resistance to airflow through the porous bed. For the porosity value of 0.375 and element diameter of 12 mm, a pressure drop of over 6 kPa was obtained, and for the porosity value of 0.39 and element diameter of 24.5 mm, the pressure drop was over 2 kPa. This relationship is particularly important with regard to the selection of appropriate air pumping equipment and from the perspectives of the exergy efficiency of the system. The amount of stored energy in the heat storage tank and the heat loss to the environment are directly related to the amount of rock material inside the heat storage tank. For a porosity value of 0.39, the maximum achieved stored energy was the lowest of the studied, and for a porosity value of 0.375, the stored heat value was the largest.

## 4. SUMMARY

Increasing climate awareness, the progressive decarbonization process and the reduction of the human carbon footprint are encouraging the development of investments and projects aimed at increasing the energy efficiency of processes and managing waste energy. The Thermal Energy Storage system presented in this paper is applicable to both micro and large-scale systems. The use of post-mining shafts is an opportunity to simultaneously utilize unused underground and above-ground infrastructure, as well as expand the power grid with large-scale electricity storage systems. Moreover, an undoubted advantage of this solution is the location of mine shafts in a large agglomeration, which will reduce energy losses resulting from its transmission over long distances.

A very important aspect in the design of a Thermal Energy Storage system is determining the type of material that is used for thermal storage. Due to the maximum possible temperature levels (Table 1), systems with different energy efficiencies could be designed. The cost-effectiveness of the design is also influenced by the density of the material as well as its price, so it is necessary to find the right optimum design that is a compromise between the cost of the system and its efficiency. Prior to the design phase, it is necessary to recognize the thermodynamic properties of the materials under study and their performance within the Thermal Energy Storage tank. The research performed indicated that due to the lowest density and average heat capacity of the materials studied, granite has the fastest and most intense physical exit loss from the storage tank. However, there was no significant effect on air pressure drop depending on the chosen accumulation materials. The porosity and granulation of the rock bed have a significant effect on the value of air pressure drop. The tested porosity values in the range of 0.375–0.39 indicated air pressure drop in the range of 2 kPa to more than 6 kPa. In addition, no significant differences were recorded in the intensity of heat transfer by the rock material. Instead, significant differences were recorded for the occurrence of physical exit loss as a function of bed porosity. This factor is extremely important in the case of designing reservoirs with a fixed temperature of the medium.

## ACKNOWLEDGMENT

Paper is financed by statutory research founds 08/050/BK_22/0258.

## REFERENCES

[1] Strielkowski W., Civín L., Tarkhanova E., Tvaronavičienė M., Petrenko Y. (2021). Renewable Energy in the Sustainable Development of Electrical Power Sector: A Review. *Energies 14*(24).

[2] REN21. 2021. Renewables 2021 Global Status Report (Paris: REN21 Secretariat). ISBN 978-3-948393-03-8. Available online: www.ren21.net (accessed on 14 February 2022).

[3] National Energy System reports. Available online: https://www.pse.pl/dane-systemowe/funkcjonowanie-kse/raporty-roczne-z-funkcjonowania-kse-za-rok/raporty-za-rok-2020 (accessed on 14 February 2022).

[4] Jurczyk M., Węcel D., Uchman W., Skorek-Osikowska A. (2022). Assessment of operational performance for an integrated "power to synthetic natural gas" system. *Energies 15*(1).

[5] Kotowicz J., Jurczyk M., Węcel D. (2021). The possibilities of cooperation between a hydrogen generator and a wind farm. *International Journal of Hydrogen Energy 46*(10).

[6] Kotowicz J., Jurczyk M (2019). Economic analysis of an installation producing hydrogen through water electrolysis. *Journal of Power Technologies 99*(3), 170–175.

[7] Bartela Ł. (2020). A hybrid energy storage system using compressed air and hydrogen as the energy carrier. *Energy* 196.

[8] Koceman A.S., Modi V. (2017). Value of pumped hydro storage in a hybrid energy generation allocation system. *Applied Energy* 205, 1202–1215.

[9] Uchman W., Skorek-Osikowska A., Jurczyk M., Węcel D. (2020). The analysis of dynamic operation of power-to-SNG system with hydrogen generator powered with renewable energy, hydrogen storage and methanation unit. *Energy* 213.

[10] Węcel D., Jurczyk M., Uchman W., Skorek-Osikowska A. (2020). Investigation on system for renewable electricity storage in small scale integrating photovoltaics, batteries, and hydrogen generator. *Energies 13*(22), 1–19.

[11] Pfeiffer W. T., Witte F., Tuschy I., Bauer S. (2021). Coupled power plant and geostorage simulations of porous media compressed air energy storage (PM-CAES). *Energy Conversion and Management*, 249.

[12] Chaychizadeh F., Dehghandorost H., Aliabadi A., Taklifi A. (2018). Stochastic dynamic simulation of a novel hybrid thermal-compressed carbon dioxide energy storage system (T-CCES) integrated with a wind farm. *Energy Conversion and Management,* 166, 500–511.

[13] Tola V., Meloni V., Spadaccini F., Cau G. (2017). Performance assessment of Adiabatic Compressed Air Energy Storage (A-CAES) power plants integrated with packed-bed thermocline storage systems. *Energy Conversion and Management,* 151, 342–356.

[14] Mehla N., Kumar A. (2021). Experimental evaluation of used engine oil based thermal energy storage coupled with novel evacuated tube solar air collector (NETAC). *Journal of Energy Storage* 2021.

[15] Liu X., Chen M., Xu Q., Gao K., Dang C., Li P., Luo Q., Zheng H., Song C., Tian Y., Yao H., Jin Y., Xuan Y., Ding Y. (2022). Bamboo derived SiC ceramics-phase change composites for efficient, rapid, and compact solar thermal energy storage. *Applied Energy* 240.

[16] Muthukumaran J., Senthil R. (2022). Experimental performance of a solar air heater using straight and spiral absorber tubes with thermal energy storage. *Journal of Energy Storage,* 45.

[17] Praveen R.P., Chandra Mouli K.V.V. (2022). Performance enhancement of parabolic trough collector solar thermal power plants with thermal energy storage capability. *Ain Shams Engineering Journal*, 13.

[18] Pachori H., Choudhary T., Sheorey T. (2022). Significance of thermal energy storage material in solar air heaters. Materials Today: Proceedings. In Press, Corrected Proof, Available online 6 January 2022.

[19] Rathore P., Gupta N., Yadav D., Shukla S., Kaul S. (2022). Thermal performance of the building envelope integrated with phase change material for thermal energy storage: an updated review. Sustainable Cities and Society 79.

[20] Andersen T., Vinkovic K., de Vries M., Kers B., Necki J., Swolkien J., Roiger A., Peters W., Chen H. (2021). Quantifying methane emissions from coal mining ventilation shafts using an unmanned aerial vehicle (UAV)-based active AirCore system. Atmospheric Environment: X 12.

[21] Zheng C., Jiang B., Xue S., Chen Z., Li H. (2019). Coalbed methane emissions and drainage methods in underground mining for mining safety and environmental benefits: A review. *Process Safety and Environmental Protection* 127, 103–124.

[22] Barbour E., Mignard E., Ding Y., Li Y.(2015). Adiabatic Compressed Air Energy Storage with packed bed thermal energy storage. *Applied Energy* 155, 804–815.

[23] Bashiri Mousavi S., Adib M., Soltani M., Razmi A.R., Nathwani J. (2021). Transient thermodynamic modeling and economic analysis of an adiabatic compressed air energy storage (A-CAES) based on cascade packed bed thermal energy storage with encapsulated phase change materials. *Energy Conversion and Management* 243.

[24] Bartela Ł., Lutyński M., Smolnik G., Waniczek S. Underground Compressed Air Storage Installation. European Patent Application, No. 20000302.8.

[25] Lee K-C., Baek W-K., Kwon H., S W-S., Yoh J.J. (2013). Analysis of melt-through process of 1.07 $\mu$m continuous wave high power laser irradiation on metal. *Journal of Mechanical Science and Technology* 27, 1745–1752.

[26] Jurczyk M., Rulik S., Bartela Ł. (2020). Thermal energy storage in rock bed – CFD analysis. *Journal od Power Technologies*, Vol. 100.

[27] Ochmann J., Rusin K., Rulik S., Bartela Ł. (2022). Identyfikacja współczynnika wnikania ciepła w procesie ładowania zasobnika Thermal Energy Storage na potrzeby adiabatycznego systemu CAES (Identification of the heat transfer coefficient in the Thermal Energy Storage charging process for the adiabatic CAES system). *Współczesne problemy ochrony środowiska i energetyki*, 147–157.

[28] Waniczek S., Ochmann J., Bartela Ł., Rulik S., Lutyński M., Brzuszkiewicz M., Kołodziej K., Smolnik G., Jurczyk M., Lipka M. (2022) Design and Construction Challenges for a Hybrid Air and Thermal Energy Storage System Built in the Post-Mining Shaft. *Journal of Thermal Science*.

[29] Labus M., Labus K. (2018). Thermal conductivity and diffusivity of fine-grained sedimentary rocks. *Journal of Thermal Analysis and Calorimetry*, 132, 1669–1676.

[30] Hartlieb P., Toifl M., Kuchar F., Meisels R., Antretter T. (2016). Thermo-physical properties of selected hard rocks and their relationto microwave-assisted comminution. *Minerals Engineering*, 91.

[31] Bindra H., Bueno P., Morris J.F., Shinnar R. (2013). Thermal analysis and exergy evaluation of packed bed thermal storage systems. *Applied Thermal Engineering 52*(2), 255–263.

[32] Bouvry B., Carrion A., Andujar J., Veron E., Ory S., Brassamin S., Echegut P., Escape C., Nahhas T., Py X., Bessada C. (2017). Mediterranean basin basalts as potential materials for thermal energy storage in concentrated solar plants, *Solar Energy Materials and Solar Cells*, 171, 50–59.

[33] Churchill S. W., Chu H. (1975). Correlating equations for laminar and turbulent free convection from a vertical plate. *International Journal of Heat Mass Transfer* 18, 1323–1329.